

Merged Four Dirac Points at the Critical Interlayer Distance in Commensurately Twisted Bilayer Graphene: the Origin of the Zero Velocity

Aya Yamada and Yasumasa Hasegawa

Graduate School of Material Science, University of Hyogo,
3-2-1 Kouto, Kamigori, Hyogo, 678-1297, Japan

(Received March 11, 2020; accepted December 3, 2020; published online January 12, 2021)

We study the commensurately-tilted bilayer graphene in the tight-binding model with changing the interlayer distance, which can be tuned by pressure. We find that at the commensurately-tilted bilayer graphene with moderate rotating angles, when the energy gap at K point is not negligible, the other Dirac points within the upper two bands move along the Γ - K - M line in the bilayer Brillouzone, when the interlayer distance is changed. The velocity at K point becomes zero due to the merging of the four Dirac points within upper two bands. This mechanism of zero velocity at K point is expected to be the origin of the magic angle with flat band at ambient pressure, at which the upper two bands are almost degenerate and the band gap at K can be neglected.

1. Introduction

Single layer graphene has a two-dimensional honeycomb structure with two sites in the unit cell. Two bands touch at the corners of the first Brillouin zone (K and K' points) in single layer graphene.¹⁾ Although a small band gap may open due to the spin-orbit coupling, it is very small and can be neglected. Spatial modulations of the potential are discussed to be important for Dirac fermions.^{2,3)} Recently, bilayer graphene with a small rotating angle (twisted bilayer graphene) attracts a lot of interest.⁴⁾ The twisted bilayer graphene has a large unit cell as the twist angle becomes small. The velocity at K point is predicted to be zero at the magic angles.⁵⁻⁹⁾ It is also shown that the bands at the charge neutral point are exactly flat when the interlayer coupling is finite only between the sites belonging the different sublattice in each layers.¹⁰⁾

When the bands become so flat that the band width or kinetic energy is in the same order as or smaller than the interaction energy between electrons, the interaction between electrons becomes important. Indeed, strongly correlated insulator phase and superconductivity in twisted bilayer graphene at the first magic angle ($\sim 1^\circ$) have been observed.^{11,12)} The magic angle is predicted to be controlled by pressure,¹³⁾ and shown experimentally.¹⁴⁾ The zero velocity at K point is a necessary condition for the flat band but not a sufficient condition. The study of the mechanism of zero velocity, however, is important to understand the magic angle in bilayer graphene. In this paper we study the condition for the zero velocity at K point.

Many theoretical studies have been done,^{3-10,13,15-21)} but there exist a lot of mysteries remain to be revealed, especially, the mechanism of zero velocity at the magic angles. Most of the previous studies have been done in the continuous model.⁶⁾ In the continuous model the unit cell is infinite. The energy gap at K point in the moiré Brillouin zone is zero. The continuous model can be jus-

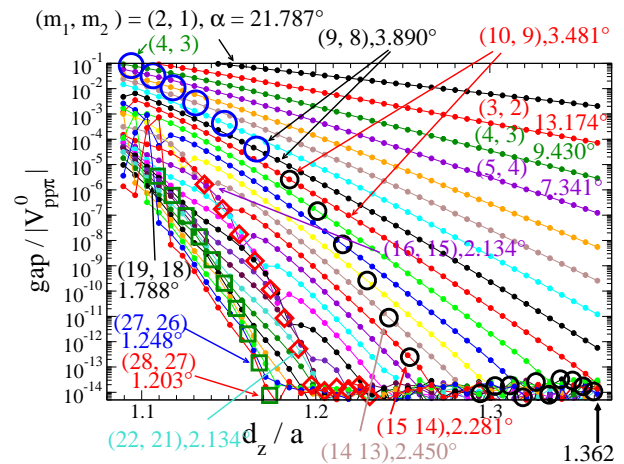


Fig. 1. (color online) Energy gap as a function of the interlayer distance for commensurately rotated angles with $(m_1, m_2) = (2, 1), (3, 2), (4, 3), \dots, (28, 27)$. The gaps smaller than $\sim 10^{-14}$ are caused by numerical errors and have no serious meanings. Large open black circles, red diamonds, and green squares are the first, second and third critical interlayer distances, where the velocity at K with $\delta_k = 0.01$ in Eq. (6) is zero as V-shaped cusps which are related to the first, second and third magic angles for the commensurately rotated bilayer graphene, respectively. Large blue circles are the critical interlayer distance, where the velocity at K with $\delta_k = 0.01$ in Eq. (6) is zero as a reversed V-shaped cusp. At the ambient pressure $d_z/a = 1.362$.

tified only in the case of small twist angles. On the other hand, the commensurately tilted bilayer graphene has a finite number of sites in the unit cell (see Appendix). The twisted bilayer graphene in the ambient pressure has the fixed interlayer distance, and the strength of the interlayer coupling with respect to the hopping integrals in the layer is constant. Then the band gap at the Dirac points is negligibly small in small twisted angles. When the twist angle is finite, a finite gap, however, exists even without the spin-orbit coupling, as shown in Fig. 1. In this figure

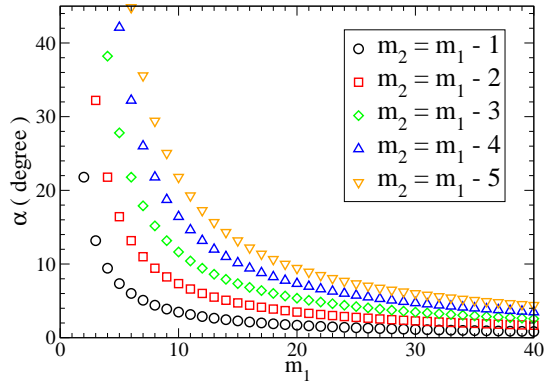


Fig. 2. (color online). Rotating angle α of the commensurately rotated bilayer graphene with m_1 and m_2 (Eq. (A-13) and Eq. (A-14)). When $m_1 - m_2$ is divisible by 3 (green diamonds), energy gap is zero.¹⁶⁾ In this paper we consider mainly $m_2 = m_1 - 1$ (black circles).

the rotating angle is taken to be commensurate, i.e., the rotating angle α is given by a pair of integers (m_1, m_2) , as shown in Fig. 2. The energy gap at the Dirac points is caused by the coupling between the distant Dirac points in the Brillouin zone for each layer,¹⁶⁾ which is neglected in the continuous model. Since the vertical axis in Fig. 1 corresponds to the strength of the coupling between K and K', Fig. 1 can be seen as the interlayer-distance and twist-angle dependences of the coupling strength of the inter-valley scattering. These dependences should be observed by experiments.

This situation is similar to the zero modes in the presence of the uniform magnetic field in the single layer graphene with anisotropic hoppings;^{22, 23)} If the hoppings between the nearest sites are anisotropic in the absence of external magnetic field, the Dirac points moves from K and K' points, but the energy gap remains zero at Dirac points unless two Dirac points merge at one of the time reversal invariant momentums, Γ and three M points.²⁴⁾ There exists the zero mode in a uniform magnetic field in single layer graphene, if the hopping between nearest sites are isotropic. The energy gap becomes finite, however, if the one of the hoppings is larger than the other two hoppings.^{22, 23)} The opening of the gap in the single-layer graphene in magnetic field with the anisotropic hoppings is shown to be caused by the coupling of two Dirac points.²³⁾

In this paper we study the commensurately twisted bilayer graphene in the tight-binding model with changing the interlayer distance. We mainly study the case $(m_1, m_2) = (m_1, m_1 - 1)$. When $m_1 - m_2$ is an integer multiple of 3, the energy gap is zero at K as shown by Mele.¹⁶⁾ We do not consider that case. We ignore the lattice relaxation, which may occur and affect the electron structure in the twisted bilayer graphene.^{18, 25, 26)}

The energy gap at ambient pressure ($d_z/a = 1.362$) is exponentially small and can be neglected when the rotating angle α is small ($\alpha \lesssim 2.134^\circ$). When the energy gap

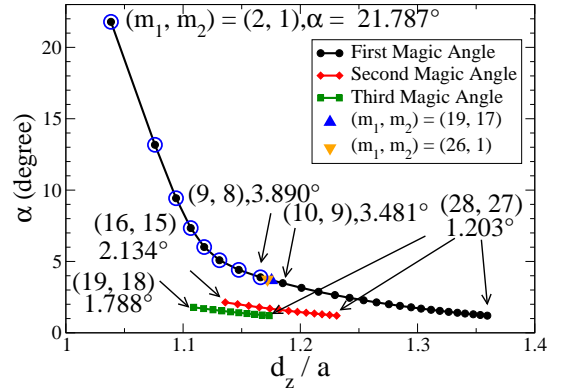


Fig. 3. (color online). First (black circles), second (red diamonds), and third (green squares) critical interlayer distances in commensurately rotated bilayer graphene with $m_2 = m_1 - 1$ ($m_1 = 2, 3, 4, \dots, 28$). These points correspond to the first, second, and third magic angles, respectively. Large blue circles show that the velocity obtained with $\delta_k = 0.01$ in Eq. (6) is zero as the reversed V-shaped cusp as a function of the interlayer distance. The blue triangle and orange downward triangle are the critical interlayer distances for $m_2 = m_1 - 2 = 17$ and $m_1 = 26$ and $m_2 = 1$ with $\alpha' = 60^\circ - \alpha$, respectively. These two points are on the smooth line of $(m_1, m_1 - 1)$.

can be neglected, each two bands are almost degenerated around K point and four bands touch at K point, which is a massless Dirac point (number of the bands are doubled, if the spin degree of freedom is taken into account). The velocity at K point becomes zero when the interlayer distance is a critical value (shown by circles in Fig. 1). We define it as the critical interlayer distance, d_{zc} , which is related to the magic angle at ambient pressure. Even when the energy gap is not negligible, the K point remains a Dirac point for upper two bands and lower two bands. In that case the velocity at K point becomes zero at a critical value of the interlayer distance. As we will show in section 3, we numerically obtain the velocity by taking the differentiation with small δ_k which we take to be 0.01. When we take a fixed value of δ_k , the interlayer-distance dependence of the velocity at K point changes from a V-shaped cusp to a reversed V-shaped cusp. Even with the finite energy gap at K point, the velocity at K point in commensurately twisted bilayer graphene becomes zero at the critical value of the interlayer distance, which we show depend continuously on the interlayer distance, as shown in Fig. 3. We find that the zero-velocity is caused by the merging of three moving Dirac points and the fixed Dirac point at K. If we take smaller value of $\delta_k = 0.001$ for example, the critical value of the interlayer distance at $(m_1, m_2) = (10, 9)$, which is identified as the V-shaped cusp with $\delta_k = 0.01$, is shown to be the reversed V-shaped cusp. We conclude that when the gap is not negligible, the cusp at the critical interlayer distance is actually a reversed V-shaped cusp caused by the merging of four Dirac point at K point.

2. Tight-binding Model in Commensurately Twisted Bilayer Graphene

We study the tight-binding model in the commensurately twisted bilayer graphene. The contents of this section have been discussed in existing literature.^{27,28)} The details are given in Appendix . The rotating angle α is given by two integers m_1 and m_2 as

$$\alpha = \arccos\left(\frac{m_1^2 + 4m_1m_2 + m_2^2}{2(m_1^2 + m_1m_2 + m_2^2)}\right). \quad (1)$$

The number of sites in the unit cell is

$$4n_0 = 4(m_1^2 + m_1m_2 + m_2^2), \quad (2)$$

i.e., n_0 A sites and n_0 B sites in the first layer, and n_0 A sites and n_0 B sites in the second layer. We plot α as a function of m_1 in Fig. 2.

The Hamiltonian is given by

$$\mathcal{H} = - \sum_{i,j} t(\mathbf{r}_i, \mathbf{r}_j) c_i^\dagger c_j, \quad (3)$$

where \mathbf{r}_i and \mathbf{r}_j are the lattice sites in the commensurately twisted bilayer graphene. The hopping matrix elements are given by

$$t(\mathbf{r}_i, \mathbf{r}_j) = V_{pp\pi}^0 \exp\left(-\frac{d-a_0}{\delta}\right) \left(1 - \left(\frac{d_z}{d}\right)^2\right) + V_{pp\sigma}^0 \exp\left(-\frac{d-d_0}{\delta}\right) \left(\frac{d_z}{d}\right)^2, \quad (4)$$

where $V_{pp\pi}^0 \approx -0.27\text{eV}$ is the transfer integral between the nearest sites in the same layer (the distance between the nearest atoms is $a_0 = a/\sqrt{3} \approx 0.142\text{nm}$), $V_{pp\sigma}^0 \approx 0.48\text{eV}$ is the transfer integral between the atoms in different layers with the same x, y coordinates at ambient pressure (the distance between the atoms is $d_0 \approx 0.335\text{nm} \approx 1.362a$), the decay length of the transfer integrals is $\delta \approx 0.184a$, and $d = |\mathbf{r}_i - \mathbf{r}_j|$ is the distance between \mathbf{r}_i and \mathbf{r}_j . We take the interlayer distance d_z as a variable parameter, which can be changed by pressure. Note that $d = \sqrt{d_z^2 + d_{xy}^2}$, if \mathbf{r}_i and \mathbf{r}_j are in the different layers, where d_{xy} is the distance projected on the plane. Interlayer transfers are large between atoms with $d_{xy} \ll d_z$, when the interlayer transfers are approximately given by

$$t(\mathbf{r}_i, \mathbf{r}_j) \approx V_{pp\sigma}^0 \exp\left(-\frac{d_z-d_0}{\delta}\right). \quad (5)$$

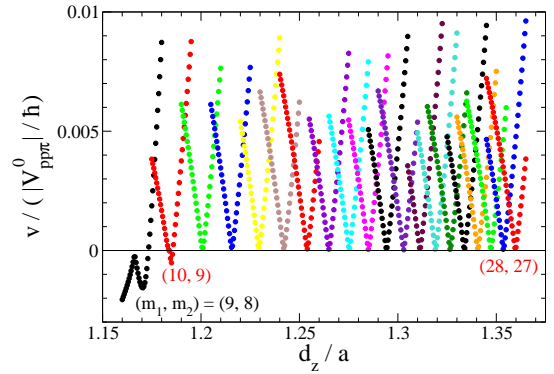
The energy gap at K point is nearly proportional to $\exp(-d_z)$ for small d_z as seen in Fig. 1.

In this paper we take a as a unit of the length, $|V_{pp\pi}^0|$ as a unit of energy, and $|V_{pp\pi}^0|a/\hbar$ as a unit of velocity. Therefore, the velocity at the K point in a single layer graphene with only nearest-neighbor hopping, $\frac{\sqrt{3}}{2}|V_{pp\pi}^0|a/\hbar$, is $\frac{\sqrt{3}}{2} = 0.866$ in the unit of $|V_{pp\pi}^0|a/\hbar$.

3. Energy Gap and the Velocity at K Point

Energy gap at K point in the commensurately rotated bilayer graphene is obtained numerically as $\epsilon_{2n_0+1}(\mathbf{K}) - \epsilon_{2n_0}(\mathbf{K})$, where $\epsilon_{2n_0+1}(\mathbf{K})$ and $\epsilon_{2n_0}(\mathbf{K})$ are the energy at K point in the $(2n_0+1)$ th band and the $2n_0$ th band

(a)



(b)

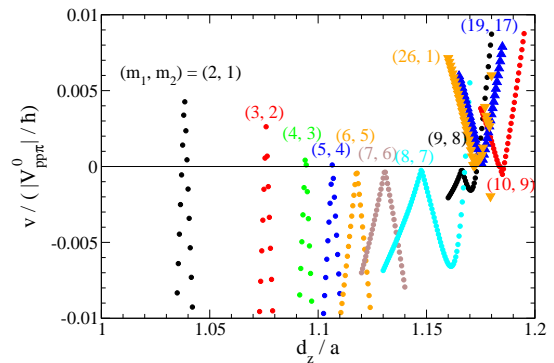


Fig. 4. (color online) Velocities in the $(2n_0+1)$ th band at K point defined in Eq. (6) with $\delta_k = 0.01$ as a function of the interlayer distance for commensurately rotated angles given by $(m_1, m_2) = (9, 8), (10, 9), \dots, (28, 27)$ (a) and $(m_1, m_2) = (2, 1), (3, 2), \dots, (9, 8)$ (b). Velocities at K point for the commensurately rotated angles given by $(m_1, m_2) = (19, 17)$ (blue triangles) and $(26, 1)$ orange downward triangles) are also plotted in (b).

from the bottom, respectively. We plot them as a function of the interlayer distance d_z in Fig. 1. When the twist angle is small ($\alpha \lesssim 3.481^\circ$, i.e. $(m_1, m_1 - 1)$ with $m_1 \geq 10$) and d_z/a is near the value at ambient pressure ($d_z/a = 1.362$), the energy gap at K point is negligibly small (smaller than the numerical error $\sim 10^{-14}$) as shown in Fig. 1.

We calculate the velocity of the $(2n_0+1)$ th band at K point as

$$v = \frac{\epsilon_{2n_0+1}((1+\delta_k)\mathbf{K}) - \epsilon_{2n_0+1}(\mathbf{K})}{\delta_k |\mathbf{K}|}, \quad (6)$$

where $\epsilon_{2n_0+1}((1+\delta_k)\mathbf{K})$ is the energy of the $(2n_0+1)$ th band (the band just above the half) at the wave number $(1+\delta_k)\mathbf{K}$, \mathbf{K} is the wave vector of K point in commensurately-twisted bilayer graphene, and δ_k is a dimensionless parameter for the numerical differentiation. We take $\delta_k = 0.01$ in the most part of the paper and take a small value in some cases. Since $\frac{3}{2}\mathbf{K}$ is one of the M points in the extended zone scheme and

$|\mathbf{K}| \equiv |\mathbf{K} - \mathbf{\Gamma}| = 2|\mathbf{M} - \mathbf{K}|$, v is also given by

$$v = \frac{\epsilon_{2n_0+1}(\mathbf{K} + 2\delta_k(\mathbf{M} - \mathbf{K})) - \epsilon_{2n_0+1}(\mathbf{K})}{2\delta_k|\mathbf{M} - \mathbf{K}|}. \quad (7)$$

In fig. 4 we plot the velocities defined by Eq. (6) with $\delta_k = 0.01$ as functions of d_z/a for $(m_1, m_1 - 1)$ ($m_1 = 2, 3, \dots, 28$), $(m_1, m_2) = (19, 17)$, and $(m_1, m_2) = (26, 1)$. In our choice of parameters, the velocity at K point (the Dirac point) in the bilayer graphene is zero when $m_1 = 28$ and $m_2 = 27$ at ambient pressure when $d_z/a = 1.362$, where a is the lattice constant in each layer and d_z is the distance between layers. The result at $m_1 = 28$ and $m_2 = 27$ is consistent with the previous results in the tight-binding approximation⁷⁾ and the continuous approximation.^{5-7,9,10)} We also find that the second and the third magic angles are obtained in the tight-binding model when the interlayer distance becomes small.

As seen in Fig. 4, there is a qualitative difference between the d_z -dependences of v near $v = 0$ between those with $m_1 \geq 10$ ($m_2 = m_1 - 1$) and those with $m_1 \leq 9$ ($m_2 = m_1 - 1$). The velocity of the upper ($(2n_0 + 1)$ th) band at K point is positive near the critical value of d_z when $m_1 \geq 10$ (V-shaped cusp), while that is negative when $m_1 \leq 9$ (reversed V-shaped cusp). We plot the velocity of the $(2n_0 + 1)$ band (upper band) calculated by Eq. (6) and the velocity of the $2n_0$ th band (lower band) calculated by

$$v' = \frac{\epsilon_{2n_0}((1 + \delta_k)\mathbf{K}) - \epsilon_{2n_0}(\mathbf{K})}{\delta_k|\mathbf{K}|}, \quad (8)$$

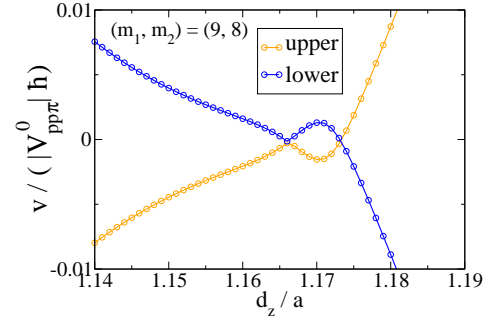
for $(m_1, m_2) = (9, 8)$ and $(10, 9)$ in Fig. 5. The velocities of the upper band v and the lower band satisfies $v = -v'$ in these regions. We discuss the $(m_1, m_2) = (9, 8)$ case and $(10, 9)$ case separately in following subsections. The case of $(m_1, m_2) = (2, 1)$ is also discussed.

3.1 $(m_1, m_2) = (9, 8)$

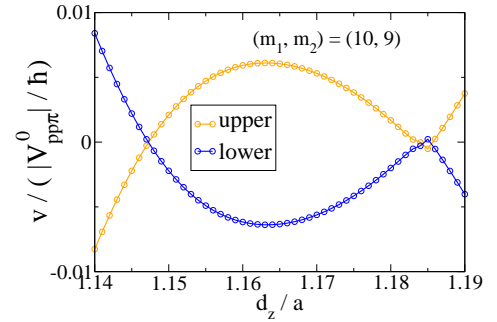
As seen in Fig. 5 (a) (orange curve), $v < 0$ at $d_z/a \lesssim 1.173$. This value of the sign-change point, however, is not a intrinsic one, but depends on the choice of δ_k . As shown in Fig. 6 (b) and (d), the Dirac point at K is not the degenerated point of four bands. The Dirac point is separated into two Dirac points of upper two bands and lower two bands due to the finite gap at K point, which has been shown by Mele.¹⁶⁾ As a result the velocity of the upper band at K point, which is positive when we take $\delta_k = 0.01$ (orange curve in Fig. 5(a)), is negative due to the small but finite energy gap when $d_z/a = 1.18$, if we take smaller value of δ_k . Therefore, the sign-change point at $d_z/a \sim 1.173$ becomes larger, if we calculate the velocity using a smaller value of δ_k . Even when $d_z/a = 1.20$, there exists a finite gap at K point, as seen in Fig. 6 (d). Therefore, the sign-change point at $d_z/a \sim 1.173$ is not intrinsic. In principle, the velocity of K point is negative (or zero) in the limit of $\delta \rightarrow 0$, if a gap between $(2n_0)$ th band and $(2n_0 + 1)$ th band cannot be neglected and there exist massless Dirac points between $(2n_0 + 1)$ th band and $(2n_0 + 2)$ th band.

On the other hand, the velocity of the upper band depends on the interlayer distance as the reversed V-shaped

(a)



(b)



(c)

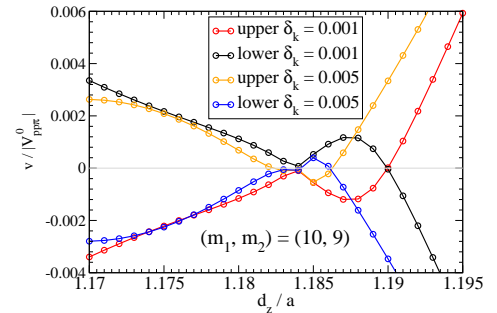


Fig. 5. (color online) Velocity in the upper ($(2n_0 + 1)$ th) band (orange) and the lower ($2n_0$ th) band (blue) at K point as a function of the interlayer distance for commensurately rotated angles given by $(m_1, m_2) = (9, 8)$ [(a)] and $(10, 9)$ [(b) and (c)]. We take $\delta_k = 0.01$ in (a) and (b). In (c) $\delta_k = 0.001$ and 0.005 are taken. The V-shaped cusp remains for $\delta_k = 0.005$ (orange circles and line), but the reversed V-shaped cusp appears for $\delta_k = 0.0001$ (red circles and line), which is similar to (a) with $(m_1, m_2) = (9, 8)$. As δ_k becomes smaller, the value of sign-change at $d_z/a \approx 1.174$ for $\delta_k = 0.01$ [(b)] comes to $d_z/a \approx 1.184$ and disappears for $\delta_k = 0.001$. The V-shaped cusp with a negative minimum value of v at $d_z/a \approx 1.185$ for $\delta_k = 0.01$ [orange points and line in (b)] becomes a reversed V-shaped cusp at $d_z/a \approx 1.184$ with the maximum value of $v = 0$ for $\delta_k = 0.001$ [red circles and line in (c)].

cusp around $d_z/a \sim 1.166$ in the case of $(m_1, m_2) = (9, 8)$ (orange curve in Fig. 5 (a)), which is also seen in the case of $m_1 \leq 9$, $m_2 = m_1 - 1$ (see Fig. 4). The reversed V-shaped cusp can be understood as follows. When the interlayer distance is close to the critical value ($d_{zc}/a \approx 1.166$ in the case of $(m_1, m_2) = (9, 8)$) there exist other Dirac points on the lines of Γ -K-M in the extended zone

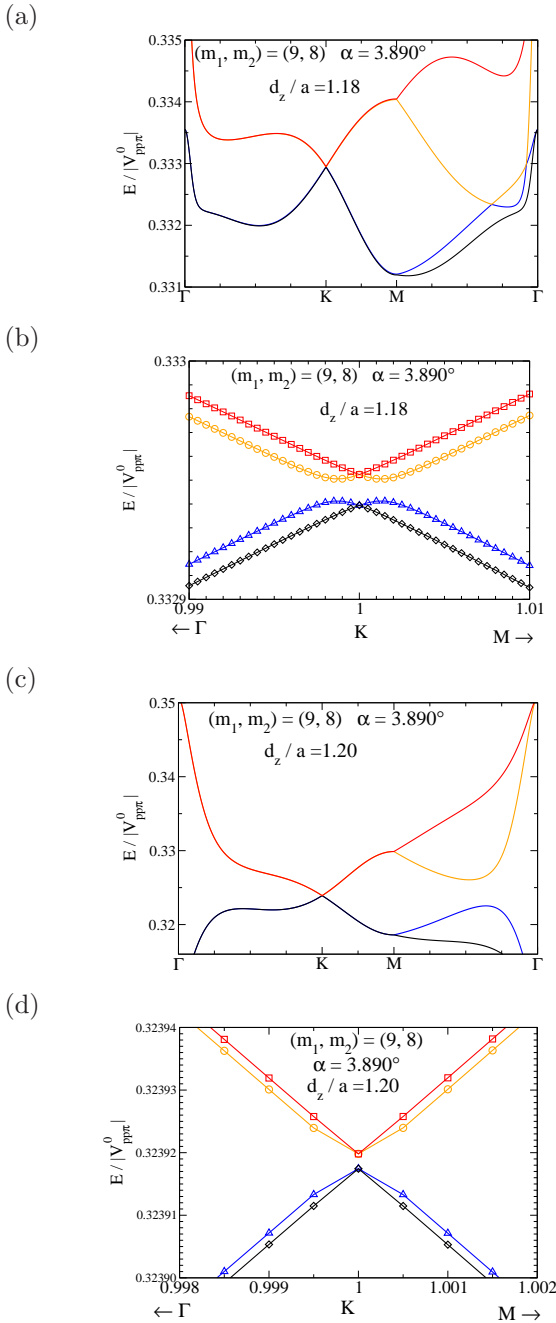


Fig. 6. (color online) Energy dispersion in the commensurately twisted bilayer graphene with $(m_1, m_2) = (9, 8)$. The interlayer distance is $d_z/a = 1.18$ [(a) and (b)], and $d_z/a = 1.20$ [(c) and (d)]. At K point the finite gap is seen in the close-up figures (b) and (d), where the momentum is scaled by $|\mathbf{K}|$. The degeneracy of the bands is lifted. The Dirac point at K is separated to two Dirac points of upper two bands ($(2n_0 + 1)$ th and $(2n_0 + 2)$ th bands) and lower two bands ($(2n_0 - 1)$ th and $2n_0$ th bands).

scheme of Brillouin zone (See Fig. 7). When $d_z/a \lesssim 1.166$ or $d_z/a \gtrsim 1.166$, three Dirac points exist near K point, as shown in Fig. 8 (a), (b) and (d). The Dirac points move as shown in Fig. 9. At $d_z/a = d_{zc}/a \approx 1.166$ four Dirac points (three moving Dirac points and one fixed Dirac point) meet at K point (Fig. 8 (c)), and at $d_z/a \approx 1.1704$ two moving Dirac point merge at M point and they disappear at $d_z/a \gtrsim 1.1704$.

Due to the $2\pi/3$ rotational symmetry and the time reversal symmetry in the twisted bilayer graphene, besides

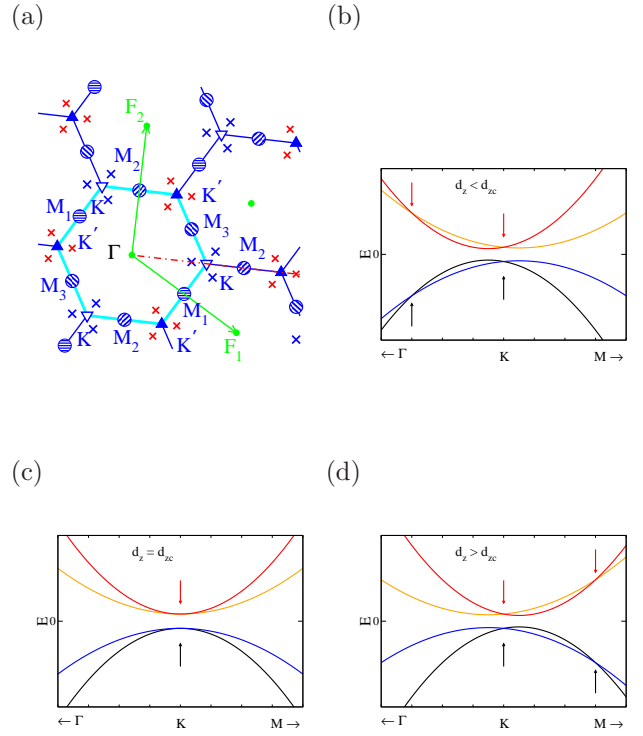


Fig. 7. (color online) (a): When the interlayer distance is close to the critical value, d_{zc} , there are six Dirac points (three red crosses and three blue crosses) in the first Brillouin zone (cyan hexagon) of the bilayer graphene. Dirac points at K (blue triangular down) and K' (filled blue triangular up) have topological number $+1$ and -1 , respectively. (b), (c), and (d): Schematic figures of the energy band near K point are shown for $d_z < d_{zc}$, $d_z = d_{zc}$, and $d_z > d_{zc}$, respectively. At $d_z = d_{zc}$ four Dirac points merge at K.

the Dirac points at K and K' points, six Dirac points should exist on three $\Gamma - K$ and three $\Gamma - K'$ lines in the first Brillouin zone in the twisted bilayer graphene, if at least one Dirac point exists in one of the $\Gamma - K$ or $\Gamma - K'$ lines (see Fig. 7). As the interlayer distance are changed to the critical value gradually, the Dirac points move to K point on the $\Gamma - K$ line and finally three moving Dirac points meet at the K point. The topological number (Berry phase) of the fixed Dirac point at K is $+1$ and that at K' is -1 and that of moving Dirac points to K (K') are -1 ($+1$). Therefore, at the critical value of the interlayer distance, where four Dirac points meet at K and K' , the topological number is -2 and $+2$ at K and K' , respectively. As a result annihilation of the Dirac points cannot happen in this case. Further change of the interlayer distance makes one Dirac points at K point and three moving Dirac points on the $K - M_j$ line, where $j = 1, 2$ and 3 . Note that $K - M_j$ line lies on the same line in $\Gamma - K$ line in the extended zone scheme. This situation is the same as the merging of Dirac points in the single-layer graphene with isotropic nearest-site hopping t and isotropic third-nearest-site hopping $t_3 \approx \frac{1}{2}t$.²⁴⁾ Since the topological number is ± 2 at the critical value of the interlayer distance, the energy depends as

$$\epsilon(\mathbf{K} + \mathbf{k}) \propto |\mathbf{k}|^2, \quad (9)$$

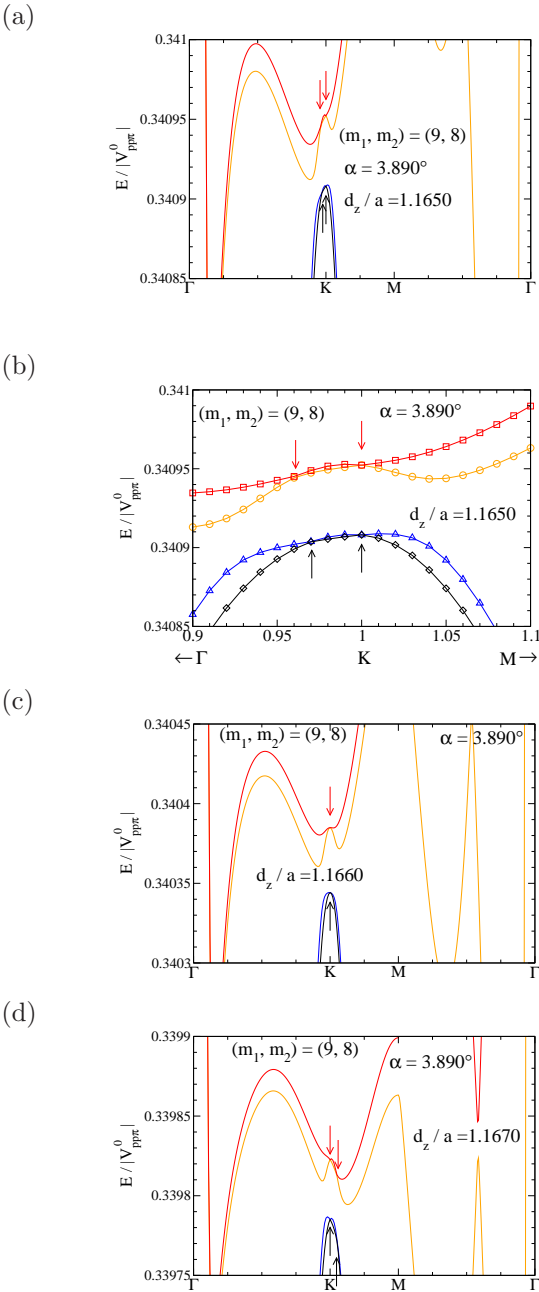


Fig. 8. (color online) Energy dispersion in the commensurately rotated bilayer graphene with $(m_1, m_2) = (9, 8)$ near the critical value of $d_{zc} = 1.1660a$. The black, blue, orange, and red lines are the $(2n_0 - 1)$ th, $(2n_0)$ th, $(2n_0 + 1)$ th, and $(2n_0 + 2)$ th bands from the bottom, respectively. The interlayer distances are taken as $1.165a$ [(a) and (b)], $1.166a$ [(c)], and $1.167a$ [(d)]. Red arrows indicate the Dirac point in the $(2n_0 + 1)$ th and $(2n_0 + 2)$ th bands, and black arrow indicate the Dirac point in the $(2n_0 - 1)$ th and $(2n_0)$ th bands.

and the velocity at K point becomes zero. Therefore, we obtain that v shows the reversed V-shaped cusp with the maximum value 0 as a function of d_z/a .

3.2 $(m_1, m_2) = (10, 9)$

The positions of sign-change and the cusp of velocity are exchanged in $(m_1, m_2) = (9, 8)$ (Fig. 5 (a)) and $(m_1, m_2) = (10, 9)$ (Fig. 5 (b)). The velocity of the $(2n_0 + 1)$ th band at K point is negative in a narrow region near $d_z/a \approx 1.185$ with V-shaped cusp when $(m_1, m_2) =$

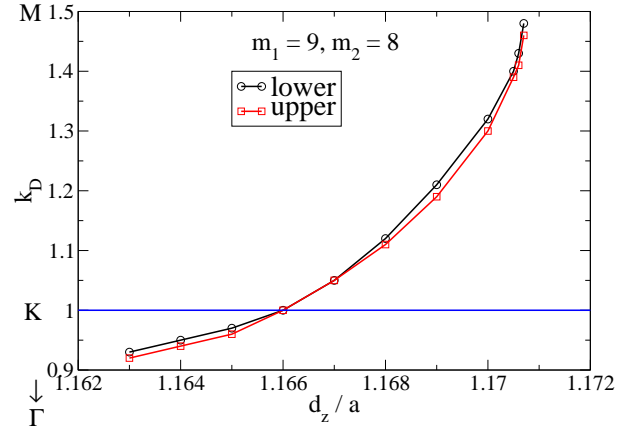


Fig. 9. (color online) The moving Dirac points for the commensurately rotated bilayer graphene with $(m_1, m_2) = (9, 8)$ as a function of interlayer distance. Four Dirac points merge at K point at $d_z/a \sim 1.1660$. Two Dirac points merge and annihilate at M point at $d_z/a \sim 1.1707$.

$(10, 9)$, as seen in Fig. 4 and Fig 5(b) orange curve, where we take $\delta_k = 0.01$. The velocity changes sign and become negative at $d_z/a \lesssim 1.147$. The value of the sign-change point $d_z/a \approx 1.147$ is not intrinsic, as in the case of $(m_1, m_2) = (9, 8)$. The V-shaped cusp also depends on δ_k , as shown in Fig 5(c) (orange and red curves). We study the V-shaped cusp near $d_z/a \approx 1.185$ in detail. We plot the energy dispersion of the bands near half-filling at $d_z/a = 1.18$ and 1.185 for $(m_1, m_2) = (10, 9)$ in Fig. 10. When we look closer near K point, the small gap between $2n_0$ th and $(2n_0 + 1)$ th bands is seen and the Dirac point separates into two Dirac points on the Γ -K-M line. Therefore, if we take δ_k small enough, the velocity of the $(2n_0 + 1)$ th band at K is negative, although it is positive at $d_z/a = 1.18$ with $\delta_k = 0.01$ (see orange curve in Fig. 5 (b)). There are other Dirac points beside K (near $0.92\mathbf{K}$ in Fig. 10 (b), red arrow), and they move toward M via K as d_z/a increases from 1.180 to 1.185 . This situation is the same as happened near $d_z/a = 1.66$ in the case of $(m_1, m_2) = (9, 8)$ (see Fig. 8). Therefore, if we take δ_k small enough, we expect the reversed V-shaped cusp in the d_z -dependence of the velocity of $(2n_0 + 1)$ th band at K in the narrow region around $d_z/a \approx 1.185$, where the velocity calculated with $\delta_k = 0.01$ is negative. At the top of the reversed V-shaped cusp, four Dirac points merge and the velocity is zero.

When the rotating angle α is smaller than 3.481° ($m_1 > 10, m_2 = m_1 - 1$), the energy gap at K is small and the upper two bands near K are almost degenerate each other. As a result, we have to take δ_k much smaller to obtain the negative region of v and reversed V-shaped cusp in d_z -dependence of v . If we take δ_k not small enough, we obtain the V-shaped cusps as in Fig. 4 (a).

We may expect that the mechanism of the V-shaped cusp in Fig. 4 (a) seen in $(m, m - 1)$ with $m \geq 10$ is the same as that of the reversed V-shaped cusp with $m \leq 9$; they are caused by the merging of four Dirac points (three moving Dirac points and the Dirac point at K). Then, the nearly flat band at the magic angle

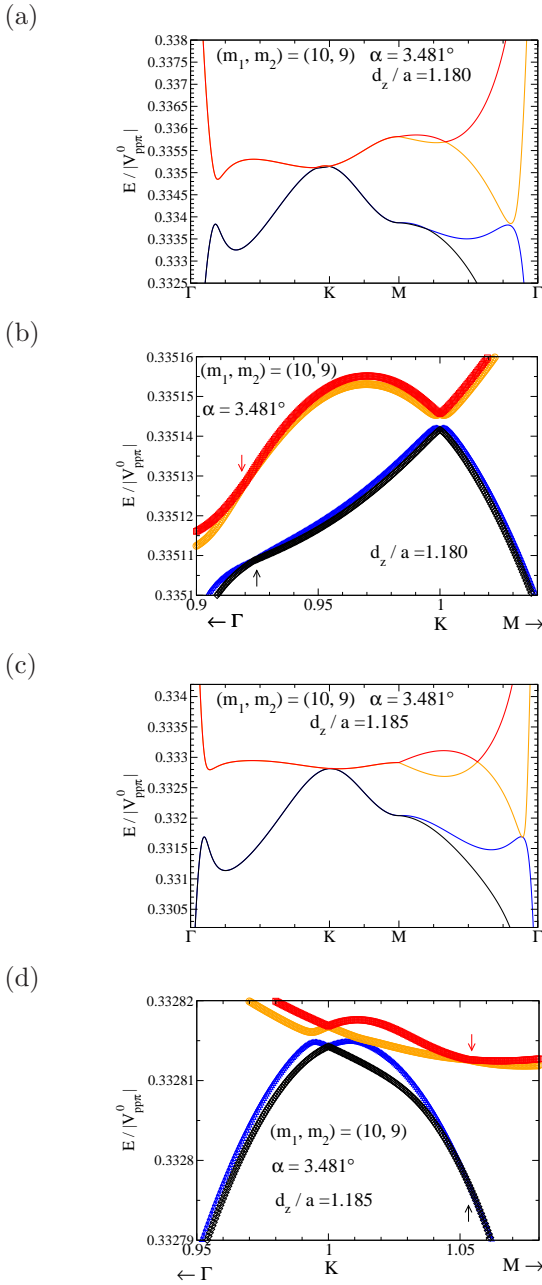


Fig. 10. (color online) Energy dispersions of $(2n_0 - 1)$ th (black), $2n_0$ th (blue), $(2n_0 + 1)$ th (orange), and $(2n_0 + 2)$ th (red) bands near K point at $d_z/d = 1.180$ [(a) and (b)] and 1.185 [(c) and (d)] for commensurately rotated angles given by $(m_1, m_2) = (10, 9)$. Red and blue arrows in (b) and (d) indicate the moving Dirac points.

at ambient pressure is thought to be the result of the merging of the four Dirac points, although it is difficult to show explicitly because of the very small energy gap at K and almost degeneracy of $(2n + 1)$ th and $(2n + 2)$ th bands.

3.3 $(m_1, m_2) = (2, 1)$

In this subsection we discuss the twisted bilayer graphene with $(m_1, m_2) = (2, 1)$ ($\alpha = 21.787^\circ$). The top of the reversed V-shaped cusp obtained by $\delta_k = 0.01$ is positive as seen in Fig. 4 (b). We show that the top of the cusp is zero as we take δ_k smaller.

In Fig. 11 we plot the energy dispersion for $(m_1, m_2) =$

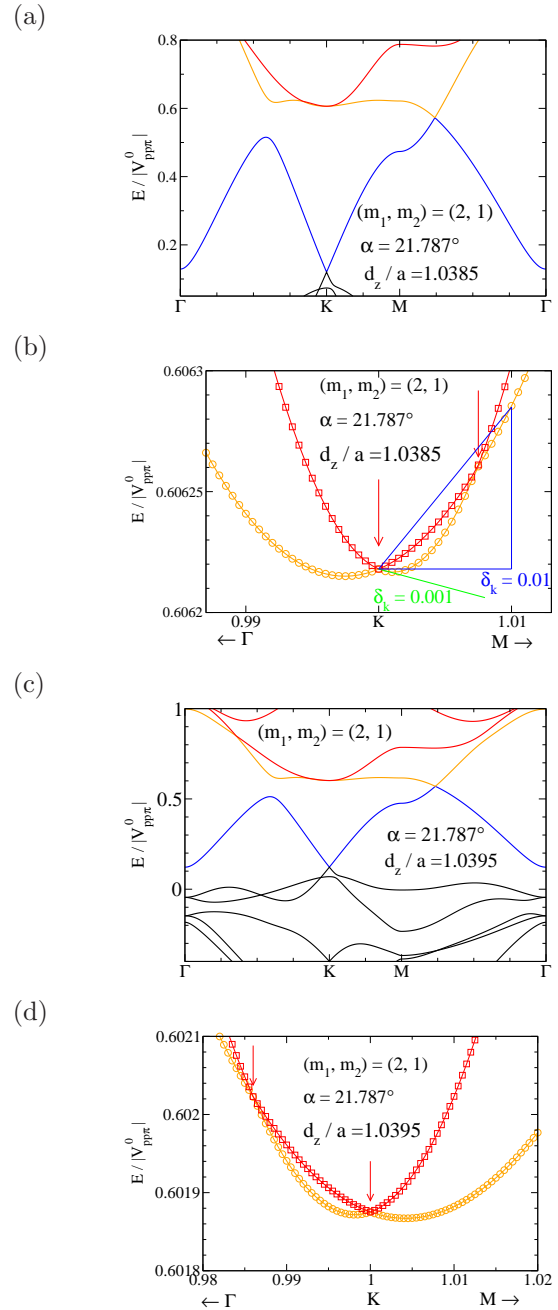


Fig. 11. (color online) Energy dispersions of $(2n_0 - 1)$ th (black), $2n_0$ th (blue), $(2n_0 + 1)$ th (orange), and $2n_0 + 2$ th (red) bands for commensurately rotated bilayer graphene with $(m_1, m_2) = (2, 1)$. The interlayer distance is $d_z/a = 1.385$ [(a) and (b)] and 1.395 [(c) and (d)]. (b) and (c) show the energy dispersion near K point. The velocity of the $(2n_0 + 1)$ th band at K point is calculated to be positive when we take $\delta_k = 0.01$ as blue lines in (b), but it is negative when we take $\delta_k \lesssim 0.001$ as shown by green line.

$(2, 1)$ near half filling at the interlayer distance $d_z/a = 1.0385$ and 1.0395 , when the velocity of the $(2n_n + 1)$ th band is small. Although v at $d_z/a = 1.0385$ obtained with $\delta_k = 0.01$ is positive, it should be negative if we take $\delta_k \lesssim 0.001$, as seen in Fig. 11 (b). There exist the moving Dirac points in the K-M line (three moving Dirac points by symmetry), and four Dirac points meet at K when d_z/a is changed. Therefore, the positive value at the top of the reversed V-shaped cusp around $d_z/a \approx 1.039$ becomes zero when we take smaller δ_k ,

If we calculate the velocity at K point in the $(2n_0 + 2)$ th band instead of the $(2n_0 + 1)$ th band, the interlayer-distance dependence of the velocity in the $(2n_0 + 2)$ th band is always V-shaped cusp and the $\delta_{\mathbf{k}}$ dependence is weak. The $\delta_{\mathbf{k}}$ -sensitivity of the velocity makes it possible to distinguish the critical values of the interlayer distance in the presence of non-negligible band gap and those in the case of negligible band gap.

The moving Dirac point in the case of $(m_1, m_2) = (2, 1)$ moves as $M \rightarrow K \rightarrow \Gamma$, as d_z/a increases around the reversed V-shaped cusp. This motion is reversal to those in the cases of $(m_1, m_2) = (9, 8)$ and $(10, 9)$. Another curious feature in $(m_1, m_2) = (2, 1)$ case is that the velocity of the $2n_0$ th band at K does not become small when that of the $(2n_0 + 1)$ th band is small, as seen in Fig. 11 (a) and (b). Since the particle-hole symmetry is broken in the commensurately rotated bilayer graphene, this asymmetry may happen, but the real reason is not clear. Despite these curious things, the critical interlayer distance defined by the zero velocity in the $(2n_0 + 1)$ th band seems to be a continuous function as a interlayer distance (see Fig. 3).

4. Discussions and Conclusion

In this paper we study the critical interlayer distance in the commensurately twisted bilayer graphene, at which the velocity of the band just above the half-filling is zero. We showed that the critical interlayer distance exists even when the energy gap at K point is not negligible. The mechanism of the zero velocity is shown to be the merging of the four Dirac points at K point.

In the continuous approximation, the energy gap at K point is neglected. The energy gap is, however, finite at K point and the degeneracy of the two bands near K point is lifted, if we take into account the coupling between K and K' points, which is in general finite in the tight binding model. In the tight binding model, the energy gap at K point is very small and can be safely neglected, only if the twist angle is small, as shown in Fig. 1. We obtain the interlayer-distance dependence of the velocity at K point in the commensurately-twisted bilayer graphene with the $4n_0$ sites in the unit cell numerically.

The velocity of the $(2n_0 + 1)$ th band at K as a function of interlayer distance becomes zero as a V-shaped cusp when $m_1 \geq 10$ and $m_2 = m_1 - 1$, while it becomes zero as a reversed V-shaped cusp when $m_1 \leq 9$ and $m_2 = m_1 - 1$, when we calculate the velocity by the numerical differentiation with $\delta_k = 0.01$ instead of taking the limit of $\delta_k \rightarrow 0$. By studying the cases with $(m_1, m_2) = (9, 8)$ and $(10, 9)$ in detail, we obtain that a reversed V-shaped cusp is caused by the merging of four Dirac point at K in both cases, if we take sufficiently small value of δ_k . At the critical interlayer distance one Dirac point with topological number ± 1 and three moving Dirac points with topological number ∓ 1 merge at K and K' points, resulting the topological number ∓ 2 . The topological number ∓ 2 means that two band touch quadratically at K and K' points, resulting the zero velocity.

This mechanism of the zero velocity at K point is shown to work in the case of small energy gap between $2n_0$ th and $(2n_0 + 1)$ th bands with $(m_1, m_2) = (10, 9)$, as

well as the cases of moderate energy gap with $(m_1, m_2) = (9, 8)$ and $(2, 1)$.

At small rotating angles, the gap between $2n_0$ th and $(2n_0 + 1)$ th bands is exponentially small, and it can be safely neglected. In that case it is difficult to distinguish the reversed V-shaped cusp and V-shaped cusp. If there is a finite gap, the velocity at K is negative when $\delta_k \rightarrow 0$ limit is taken. In that sense the zero velocity should be always realized as the reversed V-shaped cusp.

In this paper we have not concerned the flatness of the band at the magic angle, and we only study the velocity at K point. Indeed, the band is not flat at the critical interlayer distance, when the interlayer distance is small and the twist angle is not small. In the case of a small angle with negligible band gap and almost degenerate upper two bands, it is difficult to show explicitly that the flat band is caused by the merging of four Dirac points. Although we have shown that the zero velocity is caused by the merging of four Dirac points at K only for the case of moderate rotation angles, this mechanism is thought to work also for the magic angle with flat band.

Appendix: Commensurately Twisted Bilayer Graphene

We take the primitive lattice vectors of the first layer, $\mathbf{a}_1^{(1)}$ and $\mathbf{a}_2^{(1)}$, as

$$\mathbf{a}_1^{(1)} = a \begin{pmatrix} \frac{\sqrt{3}}{2} \\ -\frac{1}{2} \end{pmatrix}, \quad (\text{A}\cdot 1)$$

$$\mathbf{a}_2^{(1)} = a \begin{pmatrix} \frac{\sqrt{3}}{2} \\ \frac{1}{2} \end{pmatrix}, \quad (\text{A}\cdot 2)$$

where a is the lattice constant $a = 0.246\text{nm}$. The angle between two primitive lattice vectors are $\pi/3$;

$$\mathbf{a}_2^{(1)} = R_{\frac{\pi}{3}} \mathbf{a}_1^{(1)}, \quad (\text{A}\cdot 3)$$

where the 2D rotational matrix R_θ is given by

$$R_\theta = \begin{pmatrix} \cos \theta & -\sin \theta \\ \sin \theta & \cos \theta \end{pmatrix}. \quad (\text{A}\cdot 4)$$

Commensurately twisted bilayer graphene is labeled by two integers m_1 and m_2 . The primitive lattice vectors \mathbf{L}_1 and \mathbf{L}_2 of the commensurately twisted bilayer graphene is given by^{5, 27, 28)}

$$\mathbf{L}_1 = m_1 \mathbf{a}_1^{(1)} + m_2 \mathbf{a}_2^{(1)}, \quad (\text{A}\cdot 5)$$

$$\mathbf{L}_2 = R_{\frac{\pi}{3}} \mathbf{L}_1^{(1)} = -m_2 \mathbf{a}_1^{(1)} + (m_1 + m_2) \mathbf{a}_2^{(1)}, \quad (\text{A}\cdot 6)$$

as shown in Fig. A.1. The number of sites in the unit cell of the commensurately rotated bilayer graphene is

$$4n_0 = 4(m_1^2 + m_1 m_2 + m_2^2), \quad (\text{A}\cdot 7)$$

in the supercell, i.e. n_0 A sites and B sites in each layer.

The A sites are located at the positions

$$m_1 \mathbf{a}_1^{(1)} + m_2 \mathbf{a}_2^{(1)} \quad (\text{A}\cdot 8)$$

with integer m_1 and m_2 . We define the angle α by the angle between the vectors

$$\mathbf{L}_1 = m_1 \mathbf{a}_1^{(1)} + m_2 \mathbf{a}_2^{(1)}, \quad (\text{A}\cdot 9)$$

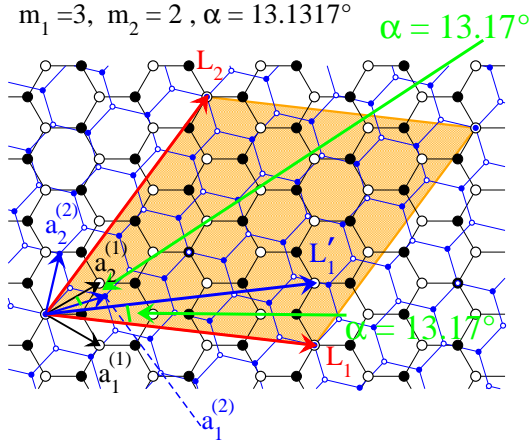


Fig. A-1. (color online). Commensurately twisted bilayer graphene with $(m_1, m_2) = (3, 2)$. Large (small) open and filled circles are A and B sublattice in the first (second) layer, respectively. The second layer is rotated by $\pi/3 - \alpha$. The orange area is the unit cell of the commensurately twisted bilayer graphene.

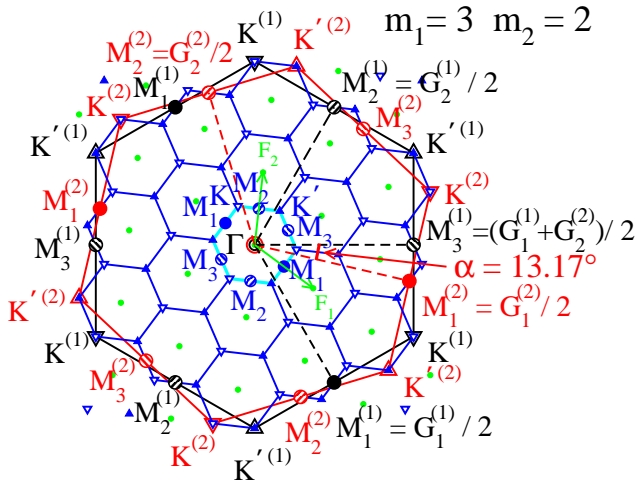


Fig. A-2. (Color online) Brillouin zone of the commensurately twisted bilayer graphene with $m_1 = 3$ and $m_2 = 2$. The large black hexagon is the first Brillouin zone of the first layer, and the large red hexagon is the first Brillouin zone of the second layer. Black triangular-down's (triangular-up's) are the K (K') points and the equivalent points of the first layer, $K^{(1)}$ ($K'^{(1)}$). Red triangular-down's (triangular-up's) are the K (K') points and the equivalent points of the second layer, $K^{(2)}$ ($K'^{(2)}$). The black circles (red circles) are the M_1, M_2 , and M_3 points of the first layer (the second layer). The green small filled circles are the Γ point and its equivalent points of the twisted bilayer graphene. The cyan hexagon at the center is the first Brillouin zone of the twisted bilayer graphene. The open blue triangular-down's and filled triangular-up's are the K and K' points (and their equivalent points) of the twisted bilayer graphene, respectively. M_1, M_2 and M_3 points are shown by the blue circles on the edge of the first Brillouin zone of the twisted bilayer graphene.

and

$$\mathbf{L}'_1 = m_2 \mathbf{a}_1^{(1)} + m_1 \mathbf{a}_2^{(1)}. \quad (\text{A}\cdot 10)$$

Two vectors have the same length

$$|\mathbf{L}_1|^2 = |\mathbf{L}'_1|^2 = a^2(m_1^2 + m_1 m_2 + m_2^2) = a^2 n_0. \quad (\text{A}\cdot 11)$$

By using

$$\mathbf{L}_1 \cdot \mathbf{L}'_1 = \frac{a^2}{2}(m_1^2 + 4m_1 m_2 + m_2^2), \quad (\text{A}\cdot 12)$$

we obtain

$$\cos \alpha = \frac{m_1^2 + 4m_1 m_2 + m_2^2}{2(m_1^2 + m_1 m_2 + m_2^2)}, \quad (\text{A}\cdot 13)$$

and

$$\sin \alpha = \frac{\sqrt{3}(m_1^2 - m_2^2)}{2(m_1^2 + m_1 m_2 + m_2^2)}, \quad (\text{A}\cdot 14)$$

We can obtain the commensurate twisted bilayer graphene by rotating the second layer either α or $\pi/3 - \alpha$. In order to obtain the Bernal stacking (AB stacking) in the limit $\alpha \rightarrow 0$, we study the $\pi/3 - \alpha$ rotation in the AA stacked bilayer graphene (α rotation in the Bernal stacked bilayer graphene) in this paper. Note that

$$\cos\left(\frac{\pi}{3} - \alpha\right) = \frac{2m_1^2 + 2m_1 m_2 - m_2^2}{2(m_1^2 + m_1 m_2 + m_2^2)}, \quad (\text{A}\cdot 15)$$

$$\sin\left(\frac{\pi}{3} - \alpha\right) = \frac{\sqrt{3}m_2(2m_1 + m_2)}{2(m_1^2 + m_1 m_2 + m_2^2)}. \quad (\text{A}\cdot 16)$$

The primitive lattice vectors of the second layer are given by rotating $\pi/3 - \alpha$;

$$\begin{aligned} \mathbf{a}_1^{(2)} &= R_{\frac{\pi}{3} - \alpha} \mathbf{a}_1^{(1)} \\ &= \frac{a}{2(m_1^2 + m_1 m_2 + m_2^2)} \begin{pmatrix} \sqrt{3}m_1(m_1 + 2m_2) \\ -m_1^2 + 2m_1 m_2 + 2m_2^2 \end{pmatrix}, \end{aligned} \quad (\text{A}\cdot 17)$$

$$\begin{aligned} \mathbf{a}_2^{(2)} &= R_{\frac{\pi}{3} - \alpha} \mathbf{a}_2^{(1)} \\ &= \frac{a}{2(m_1^2 + m_1 m_2 + m_2^2)} \begin{pmatrix} \sqrt{3}(m_1^2 - m_2^2) \\ m_1^2 + 4m_1 m_2 + m_2^2 \end{pmatrix}. \end{aligned} \quad (\text{A}\cdot 18)$$

The reciprocal Lattice vectors for the first layer ($\mathbf{G}_1^{(1)}$ and $\mathbf{G}_2^{(1)}$) and the second layer ($\mathbf{G}_1^{(2)}$ and $\mathbf{G}_2^{(2)}$) are the vectors in the wave-number space and satisfy the relations,

$$\mathbf{a}_i^{(\ell)} \cdot \mathbf{G}_j^{(\ell)} = 2\pi \delta_{i,j}, \quad (\text{A}\cdot 19)$$

and

$$\hat{\mathbf{z}} \cdot \mathbf{G}_i^{(\ell)} = 0, \quad (\text{A}\cdot 20)$$

where $i, j, \ell = 1$ or 2 and $\hat{\mathbf{z}}$ is the unit vector along the z direction. They are given by

$$\mathbf{G}_1^{(\ell)} = 2\pi \frac{\mathbf{a}_2^{(\ell)} \times \hat{\mathbf{z}}}{(\mathbf{a}_1^{(\ell)} \times \mathbf{a}_2^{(\ell)}) \cdot \hat{\mathbf{z}}}, \quad (\text{A}\cdot 21)$$

$$\mathbf{G}_2^{(\ell)} = 2\pi \frac{\hat{\mathbf{z}} \times \mathbf{a}_1^{(\ell)}}{(\mathbf{a}_1^{(\ell)} \times \mathbf{a}_2^{(\ell)}) \cdot \hat{\mathbf{z}}}. \quad (\text{A}\cdot 22)$$

We obtain

$$\mathbf{G}_1^{(1)} = \frac{2\pi}{a} \begin{pmatrix} 1 \\ \sqrt{3} \\ -1 \end{pmatrix}$$

$$= \frac{4\pi}{3a^2}(2\mathbf{a}_1 - \mathbf{a}_2), \quad (\text{A}\cdot 23)$$

$$\begin{aligned} \mathbf{G}_2^{(1)} &= \frac{2\pi}{a} \begin{pmatrix} \frac{1}{\sqrt{3}} \\ 1 \end{pmatrix} \\ &= \frac{4\pi}{3a^2}(-\mathbf{a}_1 + 2\mathbf{a}_2). \end{aligned} \quad (\text{A}\cdot 24)$$

The reciprocal Lattice vectors for the second layer, $\mathbf{G}_1^{(2)}$ and $\mathbf{G}_2^{(2)}$ are obtained by rotating $\pi/3 - \alpha$,

$$\begin{aligned} \mathbf{G}_1^{(2)} &= R_{\frac{\pi}{3}-\alpha} \mathbf{G}_1^{(1)} \\ &= \frac{2\pi}{a} \frac{1}{m_1^2 + m_1 m_2 + m_2^2} \begin{pmatrix} \frac{1}{\sqrt{3}}(m_1^2 + 4m_1 m_2 + m_2^2) \\ -(m_1^2 - m_2^2) \end{pmatrix}, \end{aligned} \quad (\text{A}\cdot 25)$$

$$\begin{aligned} \mathbf{G}_2^{(2)} &= R_{\frac{\pi}{3}-\alpha} \mathbf{G}_2^{(1)} \\ &= \frac{2\pi}{a} \frac{1}{m_1^2 + m_1 m_2 + m_2^2} \begin{pmatrix} \frac{1}{\sqrt{3}}(m_1^2 - 2m_1 m_2 - 2m_2^2) \\ m_1(m_1 + 2m_2) \end{pmatrix}. \end{aligned} \quad (\text{A}\cdot 26)$$

We write the reciprocal lattice vectors of the twisted bilayer graphene as \mathbf{F}_1 and \mathbf{F}_2 , which are given by

$$\mathbf{F}_1 = 2\pi \frac{\mathbf{L}_2 \times \hat{\mathbf{z}}}{(\mathbf{L}_1 \times \mathbf{L}_2) \cdot \hat{\mathbf{z}}}, \quad (\text{A}\cdot 27)$$

$$\mathbf{F}_2 = 2\pi \frac{\hat{\mathbf{z}} \times \mathbf{L}_1}{(\mathbf{L}_1 \times \mathbf{L}_2) \cdot \hat{\mathbf{z}}}. \quad (\text{A}\cdot 28)$$

We obtain

$$\mathbf{F}_1 = \frac{1}{m_1^2 + m_1 m_2 + m_2^2} \left((m_1 + m_2) \mathbf{G}_1^{(1)} + m_2 \mathbf{G}_2^{(1)} \right) \quad (\text{A}\cdot 29)$$

$$= \frac{4\pi}{3a^2} \frac{(2m_1 + m_2)\mathbf{a}_1 + (-m_1 + m_2)\mathbf{a}_2}{m_1^2 + m_1 m_2 + m_2^2}, \quad (\text{A}\cdot 30)$$

$$\mathbf{F}_2 = \frac{1}{m_1^2 + m_1 m_2 + m_2^2} \left(-m_2 \mathbf{G}_1^{(1)} + m_1 \mathbf{G}_2^{(1)} \right). \quad (\text{A}\cdot 31)$$

$$= \frac{4\pi}{3a^2} \frac{(-m_1 - 2m_2)\mathbf{a}_1 + (2m_1 + m_2)\mathbf{a}_2}{m_1^2 + m_1 m_2 + m_2^2}, \quad (\text{A}\cdot 32)$$

We can write Eqs. (A.29) and (A.31) as

$$\mathbf{G}_1^{(1)} = m_1 \mathbf{F}_1 - m_2 \mathbf{F}_2, \quad (\text{A}\cdot 33)$$

$$\mathbf{G}_2^{(1)} = m_2 \mathbf{F}_1 + (m_1 + m_2) \mathbf{F}_2. \quad (\text{A}\cdot 34)$$

We plot Brillouin zone in the twisted bilayer graphene with $m_1 = 3$ and $m_2 = 2$ in Fig. A.2.

In the continuous model, coupling between $K^{(1)}$ and three nearest K' (including $K'^{(2)}$) are taken into account.⁶⁾ On the other hand, the commensurately-twisted bilayer graphene has an intervalley coupling between $K^{(1)}$ and $K^{(2)}$. The intervalley coupling causes the band gap at K and K' , although it is small in the ambient

pressure.¹⁵⁾ If $m_1 - m_2 = 3n$ with integer n , the band structure near K is drastically changed.^{4,19)} In this paper we do not consider that case.

-
- 1) A. H. Castro Neto, F. Guinea, N. M. R. Peres, K. S. Novoselov, and A. K. Geim: Rev. Mod. Phys. **81** (2009) 109.
 - 2) M. Gibertini, A. Singha, V. Pellegrini, M. Polini, G. Vignale, A. Pinczuk, L. N. Pfeiffer, and K. W. West: Phys. Rev. B **79** (2009) 241406.
 - 3) C. A. Downing and M. E. Portnoi: Journal of Physics: Condensed Matter **29** (2017) 315301.
 - 4) A. V. Rozhkov, A. O. Sboychakov, A. L. Rakhmanov, and F. Nori: Phys. Rep. **648** (2016) 1.
 - 5) J. M. B. Lopes dos Santos, N. M. R. Peres, and A. H. Castro Neto: Phys. Rev. Lett. **99** (2007) 256802.
 - 6) R. Bistritzer and A. H. MacDonald: Proceedings of the National Academy of Sciences **108** (2011) 12233.
 - 7) E. Suárez Morell, J. D. Correa, P. Vargas, M. Pacheco, and Z. Barticevic: Phys. Rev. B **82** (2010) 121407.
 - 8) H. C. Po, L. Zou, A. Vishwanath, and T. Senthil: Phys. Rev. X **8** (2018) 031089.
 - 9) K. Hejazi, C. Liu, H. Shapourian, X. Chen, and L. Balents: Phys. Rev. B **99** (2019) 035111.
 - 10) G. Tarnopolsky, A. J. Kruchkov, and A. Vishwanath: Phys. Rev. Lett. **122** (2019) 106405.
 - 11) Y. Cao, V. Fatemi, A. Demir, S. Fang, S. L. Tomarken, J. Y. Luo, J. D. Sanchez-Yamagishi, K. Watanabe, T. Taniguchi, E. Kaxiras, R. C. Ashoori, and P. Jarillo-Herrero: Nature **556** (2018) 80.
 - 12) Y. Cao, V. Fatemi, S. Fang, K. Watanabe, T. Taniguchi, E. Kaxiras, and P. Jarillo-Herrero: Nature **556** (2018) 43.
 - 13) S. Carr, S. Fang, P. Jarillo-Herrero, and E. Kaxiras: Phys. Rev. B **98** (2018) 085144.
 - 14) M. Yankowitz, S. Chen, H. Polshyn, Y. Zhang, K. Watanabe, T. Taniguchi, D. Graf, A. F. Young, and C. R. Dean: Science **363** (2019) 1059.
 - 15) S. Shallcross, S. Sharma, and O. A. Pankratov: Phys. Rev. Lett. **101** (2008) 056803.
 - 16) E. J. Mele: Phys. Rev. B **81** (2010) 161405.
 - 17) S. Shallcross, S. Sharma, E. Kandelaki, and O. A. Pankratov: Phys. Rev. B **81** (2010) 165105.
 - 18) K. Uchida, S. Furuya, J.-I. Iwata, and A. Oshiyama: Phys. Rev. B **90** (2014) 155451.
 - 19) A. O. Sboychakov, A. L. Rakhmanov, A. V. Rozhkov, and F. Nori: Phys. Rev. B **92** (2015) 075402.
 - 20) A. V. Rozhkov, A. O. Sboychakov, A. L. Rakhmanov, and F. Nori: Phys. Rev. B **95** (2017) 045119.
 - 21) T. M. R. Wolf, J. L. Lado, G. Blatter, and O. Zilberberg: Phys. Rev. Lett. **123** (2019) 096802.
 - 22) Y. Hasegawa and M. Kohmoto: Phys. Rev. B **74** (2006) 155415.
 - 23) K. Esaki, M. Sato, M. Kohmoto, and B. I. Halperin: Phys. Rev. B **80** (2009) 125405.
 - 24) Y. Hasegawa and K. Kishigi: Phys. Rev. B **86** (2012) 165430.
 - 25) A. M. Popov, I. V. Lebedeva, A. A. Knizhnik, Y. E. Lozovik, and B. V. Potapkin: Phys. Rev. B **84** (2011) 045404.
 - 26) N. N. T. Nam and M. Koshino: Phys. Rev. B **96** (2017) 075311.
 - 27) P. Moon and M. Koshino: Phys. Rev. B **85** (2012) 195458.
 - 28) Y. Hasegawa and M. Kohmoto: Phys. Rev. B **88** (2013) 125426.